Integrated assessment for groundwater quality and flood vulnerability in coal mining regions

Krishna Das[1] · Ganesh Chandra Dhal[1] · Ajay S. Kalamdhad[2]

Abstract

Coal mining activities greatly damage water resources, explicitly concerning water quality. The adverse effects of coal mining and potential routes for contaminants to migrate, either through surface water or infiltration, into the groundwater table. Dealing with pollution from coal mining operations is a significant surface water contamination concern. Consequently, surface water resources get contaminated, harming nearby agricultural areas, drinking water sources, and aquatic habitats. Moreover, the percolation process connected with coal mining could alter groundwater quality. Subsurface water sources can get contaminated by toxins generated during mining activities that infiltrate the soil and reach the groundwater table. The aims of this study are the creation of models and the provision of proposals for corrective measures. Twenty-five scenarios were simulated using MODFLOW; according to the percolation percentage and contamination, 35% of the study area, i.e., the middle of the research area, was the most affected. About 38.08% of the area around the mining zones surrounding Margherita is prone to floods. Agricultural areas, known for applying chemical fertilizers, are particularly vulnerable, generating a risk of pollution to surrounding water bodies during flooding. The outputs of this research contribute to identifying and assessing flood-vulnerable regions, enabling focused measures for flood risk reduction, and strengthening water resource management.

Keywords Coal mining · Surface water contamination · Groundwater percolation · Flood vulnerability · Contaminant transport

Introduction

Flood is one of the most catastrophic natural tragedies in terms of economic devastation. The most severe repercussions of floods include individuals losing their residences, valuables, and vital infrastructures such as hospitals and senior care centers. During disasters, losing electricity and mobile communication is common, hindering daily living and safety access (Jaxa-Rozen et al. 2019;

Zhao et al. 2022). Human interference with natural water bodies has increased due to extensive mining operations, soil erosion, the growth of pavement surface for housing and industrialization, the deterioration of the flora in the watershed area, and improper land use change. A significant quantity of chemical fertilizers is likely to penetrate surrounding rivers, streams, lakes, and groundwater during the inundation of agricultural areas (Zhang et al. 2022). Floods represent a recurrent and widespread natural calamity of considerable magnitude on a global scale. Historically, these occurrences have been predominantly triggered by excessive precipitation and unfavorable geographical conditions, resulting in significant human casualties and extensive economic ramifications. Addressing this challenge necessitates the meticulous identification and classification of flood-prone areas, which are imperative for effective flood management strategies and informed risk assessment protocols (Ganji et al. 2022; Lenin Sundar et al. 2022; Osei et al. 2021). These interventions include but are not limited to extensive mining

✉ Krishna Das
p21ce002@nitm.ac.in

Ganesh Chandra Dhal
ganeshdhal@nitm.ac.in

1 Department of Civil Engineering, National Institute of Technology Meghalaya, Shillong, Meghalaya, India

2 Department of Civil Engineering, Indian Institute of Technology Guwahati, Guwahati, Assam, India

activities, accelerated soil erosion, expansion of urban and industrial areas leading to increased impermeable surfaces, degradation of vegetative cover in watershed regions, and inappropriate land-use alterations.

Consequently, the susceptibility to inundation has markedly escalated, culminating in frequent catastrophic inundations. Notably, groundwater constitutes a primary water source, crucial for fulfilling escalating demands stemming from population growth, urban expansion, industrialization, and agricultural needs, particularly during periods of drought (Sarker et al. 2022). However, the unsustainable reliance on groundwater resources has led to a rapid decline in groundwater levels, exacerbating the situation by causing the depletion of wells and aquifers. While groundwater remains vital for potable water supply, particularly in rural settings and for agricultural irrigation purposes, its quality and availability are jeopardized due to contamination and overexploitation. Thus, comprehensive measures are imperative to mitigate the adverse impacts of human-induced alterations on water resources and to safeguard both human well-being and environmental sustainability. Groundwater is the main fundamental resource for meeting the needs of the population in India (Jerin et al. 2023; Mendoza et al. 2023; Wei et al. 2019). The country's replenishable groundwater potential is estimated at 432 billion cubic meters. The overexploitation of groundwater increases groundwater withdrawals nationwide. The contamination of groundwater is caused by introducing contaminants owing to groundwater overexploitation. Groundwater contamination may have geological or anthropogenic sources (Kareemuddin and Rusthum 2015). Human sources include wastewater discharge into water bodies and agricultural leftovers' runoff. Human activities may be the principal source of groundwater contamination in a city.

Heavy metals are ubiquitous, non-biodegradable, and frequently toxic contaminants of groundwater. The groundwater within the region has been subject to detrimental impacts resulting from various anthropogenic activities, notably the discharge of industrial and sanitary effluents, along with the runoff from agricultural irrigation practices (Kimanzi and Wishitemi 2001). Due to the near-riverbank dumping of pollutants, groundwater quality management and flood risk reduction in coal-mining districts are frequently delayed by significant barriers. This is particularly evident in the area under study, covering coal mines and their environs (Wei and Bailey 2021). Consequently, it is essential to investigate the contamination of the city's groundwater. For efficient environmental management and reducing the effects of coal mining on water resources, it is crucial to comprehend the routes taken by pollutants from coal mines (Xing et al. 2023).

Groundwater contamination prediction commonly employs three general approaches: index-based, statistical-based, and simulation-based models. Among these, the MODFLOW model is a simulation-based tool widely utilized for such predictions (Sivakumar et al. 2022). Visual MODFLOW, a sophisticated software tool for groundwater flow and contaminant transport modeling, offers versatile applications across various sectors. These include but are not limited to agriculture, airfields, constructed wetlands, climate change research, drought evaluations, environmental impact assessments (EIA), landfill management, and mining operations (Sathe and Mahanta 2019). Functioning as the Graphical User Interface (GUI) for the MODULAR FINITE DIFFERENCE FLOW MODEL, Visual MODFLOW streamlines the model implementation and operation process, facilitating users in efficiently conducting complex simulations (Lazzarin et al. 2022). Remarkably, the adoption of modeling software, particularly Visual MODFLOW, is more widespread in Middle Eastern and Asian nations than in other geographical regions (Kim and Ko 2023; Langlois et al. 2023; Rafiei and Nejadhashemi 2023). This heightened prevalence can be attributed to several factors, including the growing recognition of the importance of groundwater management in these regions due to water scarcity issues, increasing environmental concerns stemming from rapid industrialization and urbanization, and the availability of expertise in groundwater modeling within academic and research institutions (Singh and Singh 2019). The MODFLOW model was employed in the investigation to predict groundwater contamination (Fig. 1). Given the insights garnered from this predictive analysis, it is essential to implement proactive measures to regulate and manage groundwater usage to mitigate potential contamination risks.

Overall, this work introduces a new method to tackle the intricate environmental issues encountered in coal mining areas by combining models for evaluating groundwater quality and assessing susceptibility to flooding. This study thoroughly explains the relationship between groundwater pollution and flood vulnerability by integrating hydrological dynamics and mining consequences. This study makes a substantial addition to the field of environmental science and engineering by providing a foundation for comprehensive approaches to reduce the negative impacts of coal mining on water resources and flood-prone regions. Incorporating groundwater quality modeling and flood vulnerability assessment, this work delivers valuable insights into water resource management (Fig. 2). The findings of these simulations suggest that the central portion of the research area is most seriously affected, underlining the necessity to establish effective regulatory measures to safeguard the region's water supplies. In addition to groundwater purity concerns, the Margherita region is especially susceptible to flooding due to its high mining activities and bad land-use changes. A GIS-based method incorporating Digital Elevation Models (DEMs) was utilized to evaluate flood risk. A flood vulnerability map was generated using ArcGIS to construct a network of streamflow and local slope

Fig. 1 Process of the flow of contaminants via surface runoff and percolation
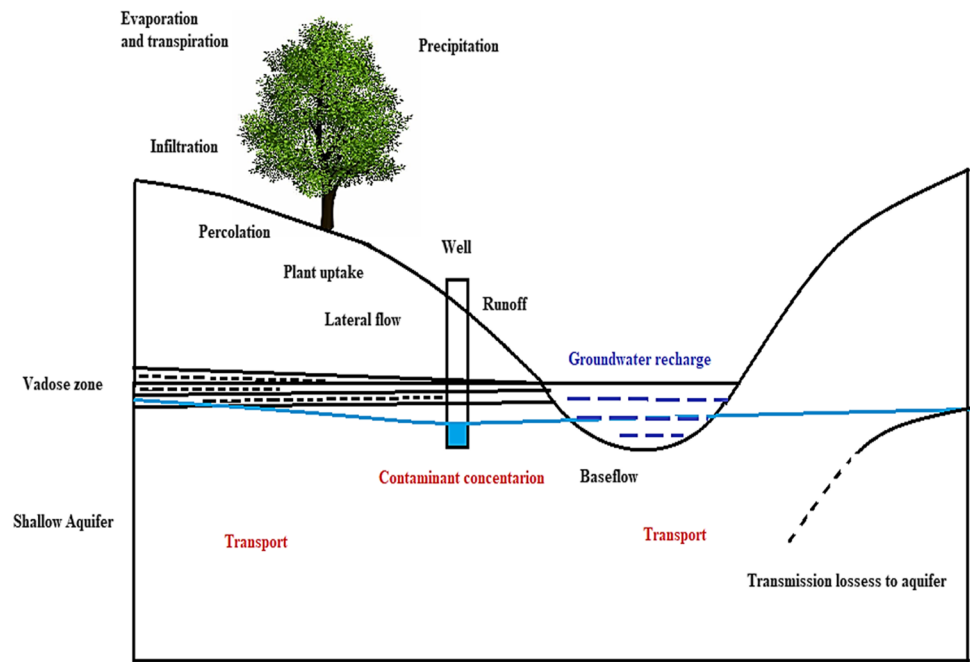
Fig. 2 An example of flood damages in the study area

variables. Agricultural areas, known for applying chemical fertilizers, constitute a substantial risk of contaminating adjacent water bodies during flood disasters. Incorporating groundwater quality modeling and flood vulnerability assessment, this work delivers valuable insights into water resource management.

The study area

Margherita is derived from the Italian monarch and dates back to the late nineteenth century as a token of appreciation for the Italian Chief Engineer of a rail segment, Chevalier R Paginini, who oversaw the construction. Margherita was renowned for its coal mines, which the British heavily developed. Coal India Limited has the most significant industrial facility in this city. The municipality is known as Coal Queen due to its prominence
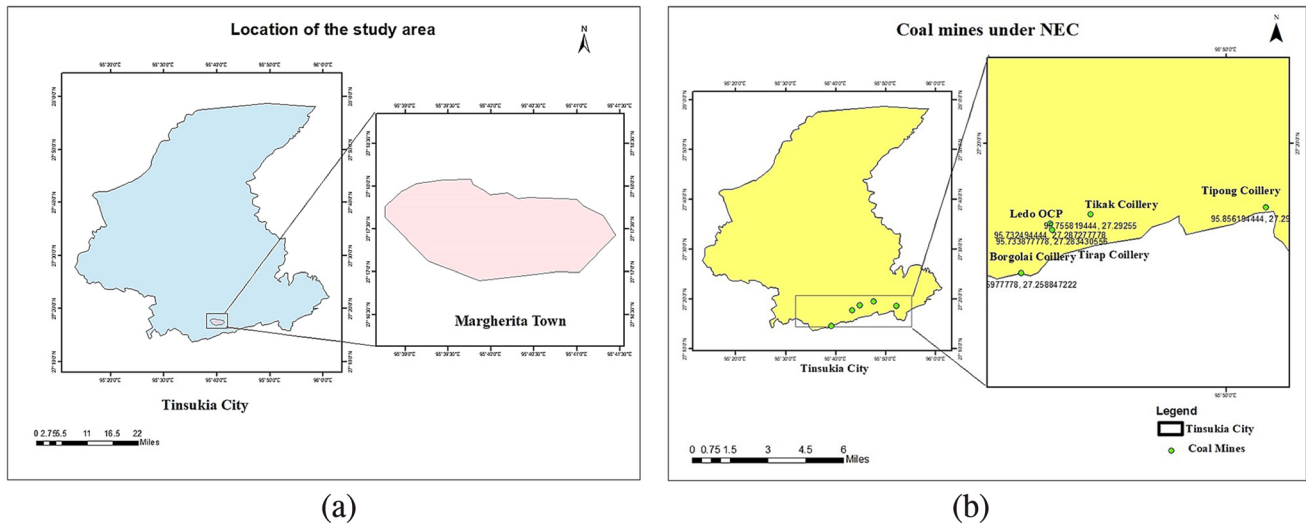
(a)   (b)

Fig. 3 **a** The study area.**b** Coal mines under North Eastern Coalfields (NEC)

in the coal industry (Fig. 3). The municipality of Margherita has been designated as the mining hub for neighboring mines. It is located in the Tinsukia district, which, as of 2011, had a population of 26,914.

Utilizing monthly rainfall data sourced from the Indian Meteorological Department spanning the years 2003 to 2021, the precipitation patterns within the study area were meticulously examined. Over the specified duration, a discernible consistency in the distribution of precipitation within the study area was observed (Fig. 4). The maximum recorded rainfall during this period peaked at approximately 1297 mm. Notably, June emerged as the period characterized by the most substantial precipitation levels, whereas January and February exhibited the least precipitation. Conversely, the below-average quantity of precipitation observed in January and February indicates seasonal variation in rainfall distribution. There are concerns about the area's ability to endure

floods due to significant changes in precipitation patterns that have been seen. Due to the potential for excessive precipitation, especially during peak months, there is a risk of increased flooding and more severe flooding in the researched region.

Materials and methods

Data collection

This study's methodology comprises several essential stages: data acquisition, analysis, model development, model calibration, results interpretation, and discussion. The primary tool utilized for predicting groundwater quality in this investigation is MODFLOW. Comprehensive data on groundwater levels, quality parameters, and
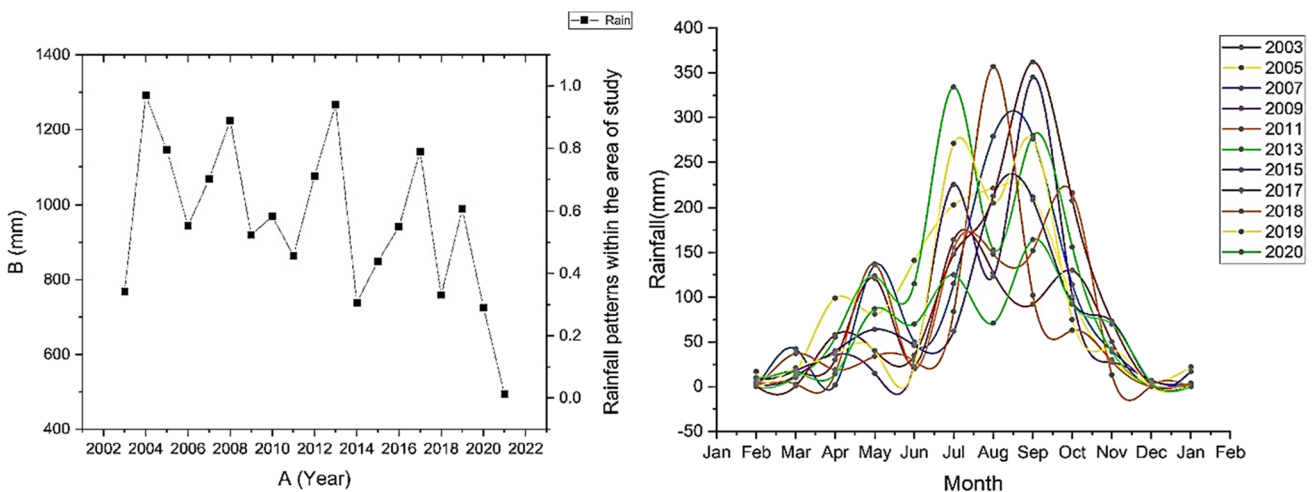

Fig. 4 Rainfall pattern in the area

Table 1 Steps in the data analysis process

Step	Description
a) Software and tools used	ESRI ArcGIS 10.8 software, surface tools, and Arc Hydro tool extensions were used to produce different layers and generate maps. This allowed for a thorough analysis of all relevant data
b) Identifying and defining flood-prone regions	The process included many phases, such as obtaining secondary data, processing it, and evaluating the acquired data to determine locations prone to flooding
c) Data acquisition	The acquiring data entailed importing a Digital Elevation Model (DEM) into the ArcGIS software, where the spatial resolution was set at 20 m (with a pixel size of 20 m × 20 m)
d) Data preparation	The data preparation for evaluating regions at risk of flooding in the study area's DEM included a sequence of procedures to provide the required data for analysis. Before conducting hydrological analysis, the data was processed using the ArcGIS program

environmental factors were initially collected from field measurements, historical records, and scientific databases (Table 1). This data was then subjected to rigorous analysis to identify trends, correlations, and potential anomalies, employing statistical tools and software to ensure accuracy and reliability. Using the analyzed data, a groundwater flow model was developed in MODFLOW, defining parameters such as boundary conditions, hydraulic properties, and initial conditions. The model was subsequently calibrated to align with observed data, and the results were interpreted to understand groundwater quality dynamics. Finally, the findings were discussed in the context of existing literature, and implications for future research and management practices were considered.

Assessment of groundwater quality by MODFLOW

The governing flow equation for three-dimensional saturated flow in porous media is articulated as follows:

$$\partial \; \partial x \; [\; kx \; \partial h \; \partial x \;] + \partial \partial x [\; ky \; \partial h \; \partial y \;] + \; \partial \; \partial z \; [\; ky \; \partial h \; \partial z \;] \pm Q = [S_s h_t]$$ (1)

In the context provided, the symbols kx, ky, and kz represent the anticipated hydraulic conductivities along the x, y, and z axes, respectively, expressed in meters per second (m/s). The variable h denotes the Head Piezometric, measured in meters (m), as a crucial indicator of groundwater elevation within the system. Additionally, the symbol Q represents the volumetric flux per unit volume, encapsulating any source or sink terms within the system. Q is dimensionally expressed in units of time (T) raised to the power of negative one (T^{-1}), signifying the volumetric flow rate per unit volume over time. Ss denotes The Specific storage coefficient, which is defined as the volume of water discharged from storage per unit change in head per unit volume of porous material, with dimensions of length to the power of negative one multiplied by time ($L^{-1} T$) and t represents time in seconds (s). Various boundary conditions are specified in the model, including those related to rivers, lakes, pumping wells, evaporation data, and recharge (Esfahani et al. 2021). These boundary conditions are crucial in simulating the model domain's groundwater flow and transport processes.

Data analysis

During the duration of the research, i.e., 6 months, collected data and samples are analyzed. Groundwater samples were systematically collected from wells and subjected to comprehensive analysis encompassing various quality parameters (Table 2). These parameters included pH, TDS, electrical conductivity (EC), total hardness (TH), chloride (Cl), alkalinity, sodium (Na^+), calcium (Ca^{2+}), magnesium (Mg^{2+}), nitrate (NO_3^-), and Sulfates (SO_4^{2-}).

A significant dataset of 2500 samples was collected over two pre-monsoon and two post-monsoon seasons. This dataset was subjected to thorough statistical analysis. Several preprocessing procedures, such as outlier filtering, normalization, and data transformation, guarantee the integrity and consistency of the data. Eliminated abnormal data points that deviated more than three standard deviations from the average, standardized the data to a standard scale, and adjusted key variables to account for asymmetry. The meticulous preprocessing and analytical methodolo-

Table 2 Initial characterization of the groundwater

Parameter	Range	Permissible range
pH	7.0 to 8.6	6.5 to 8.5
Electrical conductivity	280 to 8250 (mS/cm)	< 1500 μS/cm
Total dissolved solids (TDS)	196 to 5775 (mg/l)	< 1000 mg/l
Total hardness (TH)	80 to 1700 (mg/l)	100 to 500 mg/l
Sulfate (SO_4^{2-})	6 to 1000 (mg/l)	< 500 mg/l
Nitrate (NO_3^-)	11 to 655 (mg/l)	< 50 mg/l

gies are used to guarantee the robustness and reliability of

results. This analytical process entailed the determination of essential statistical parameters such as minimum, maximum, mean, and standard deviation values for each tested parameter, providing valuable insights into the groundwater quality dynamics within the studied area across different temporal contexts. TDS, EC, TH, calcium, magnesium, alkalinity, and chloride values were higher post-monsoon than pre-monsoon. Sulfates decreased as pH values decreased. The sodium concentrations before and after the monsoon did not differ significantly.

Model conceptualization

The initial phase of developing a groundwater flow model involves delineating the area of interest and defining the flow boundary conditions (You et al. 2023). In this process, certain assumptions were made to conceptualize the groundwater flow regions. Firstly, a data exchange format (DXF) file was imported, containing a scanned and digitized base map that serves as the foundation for the model (refer to Table 1 for details). Subsequently, the model grid was established, comprising 50 rows and columns. The total vertical extent of the model was assumed to be 75 m, with the following distribution (Table 3):

- The topmost layer, representing the upper boundary of the model, was positioned at an elevation of 0 m.
- The subsequent layers were arranged uniformly, with each layer extending downwards by a height of 1.5 m.

These assumptions form the basis for the spatial and vertical discretization of the groundwater flow model, facilitating the subsequent implementation of boundary conditions and simulation of groundwater flow dynamics within the defined study area.

The table provides a thorough summary of several strata in a hydrogeological system, clearly outlining their unique features and properties. Each layer is classified into specific categories with distinct characteristics that clarify how it

behaves regarding water movement and storage. The features column concisely describes whether a layer is confined or unconfined, indicating its association with surface water and the geological formations in its vicinity. In addition, the properties column provides detailed information on characteristics such as hydraulic conductivity, specific yield, and transmissivity, which significantly impact the flow of water inside each layer. The inclusion of variable-specific yield and transmissivity indicates the presence of geographical or temporal variations in water storage and transmission capabilities, highlighting the intricate interaction of geological, hydrological, and environmental elements that shape the hydrogeological system. In summary, this tabular representation is an excellent tool for comprehending the varied characteristics of hydrogeological strata and their crucial influence on groundwater dynamics and resource management (Table 4). The following categories were considered for this study:

The implementation of the groundwater flow model involved several critical steps and considerations. Initially, ASCII files containing well elevations relative to the Mean Sea Level were transmitted to each model stratum, facilitating the integration of well data into the model (Duran and Gill 2021). Pumping rates from approximately 20 pumping wells were estimated based on their geographical locations and intended water usage. In addition to pumping wells, head observation wells were strategically located within the study area. These wells, serving dual roles as concentration observation points, were equipped to monitor water levels and parameter concentrations. Data regarding head variations, parameter concentrations, and observation well elevations were meticulously inputted for each well, as detailed in Table 3. The model systematically recorded and assigned concentration values for all parameters at each observation site for every time step during transport simulations. Furthermore, various hydrogeological characteristics were defined for the model, encompassing parameters such as conductivity, storage coefficients, initial heads, and dispersion properties. Horizontal and vertical conductivity values were meticulously inputted and adjusted cell by cell

Table 3 Layer characteristics and properties

Layer	Type	Characteristics	Properties
Layer 1	Type 1	Unconfined	- Single hydraulic conductivity - Variable specific yield (S)
Layer 2	Type 3	Confined/unconfined	- Variable transmissivity (T) - Variable specific yield (S)
Layer 3	Type 2	Confined/unconfined	- Variable transmissivity (T) - Variable specific yield (S) - Variable specific yield (S)
Layer 4	Type 4	Confined/unconfined	- Variable transmissivity (T) - Variable specific yield (S)

Table 4 Parameters and units

Parameter	Unit
Length	Meter (m)
Time	Days
Velocity	Meters per second (m/s)
Conductivity	Siemens per meter (S/m)
Pumping rate	Cubic meters per day (m³/day)
Annual recharge	Millimeters (mm)
Mass	Kilogram (kg)
Concentration	Milligrams per liter (mg/L)

to reflect the geological heterogeneity of the study area. The influence of soil properties, including porosity, was acknowledged due to their significant impact on hydrological attributes such as hydraulic conductivity and electrical resistivity.

Once these features were defined, different boundary requirements were explicitly stated. Constant head borders were used to replicate the impact of neighboring water bodies on the northern and eastern limits of the research region. The recharge borders were primarily situated in the middle and western sections of the research area, which align with areas experiencing substantial rainfall infiltration and groundwater replenishment. In addition, river borders were established along the primary river that runs through the research area, and evapotranspiration limits were designated in regions with substantial vegetation, including water loss caused by plant absorption and evaporation. The precise boundary conditions enabled an accurate simulation of the hydrological processes in the research region.

After defining these properties, various boundary conditions were specified, including constant head, river, recharge, and evapotranspiration boundaries, among others (Table 5). These boundary conditions are crucial for executing MODFLOW simulations accurately and ensuring realistic representations of groundwater flow and transport processes within the hydrogeological model (M. Jibhakate et al. 2023). The research area was further partitioned into seven distinct zones, delineated based on variations in recharge and evapotranspiration patterns (Fig. 5). Zone budget analysis, an integral component of the modeling process, involved computing sub-regional water budgets utilizing MODFLOW simulation results. These budgets were derived through cell-by-cell flow computations, providing insights into groundwater fluxes and storage dynamics within each defined zone. After inputting all pertinent data and specifications, the model was prepared for execution within the module. The initial step of the execution phase entailed selecting either a steady-state or transient-state simulation, depending on the nature of the hydrological investigation being conducted. This preparatory phase laid the groundwork for subsequent analysis and assessment within the hydrogeological modeling framework.

These values indicate how nitrate moves with the same velocity as groundwater and spreads from its source. The molecular diffusion coefficient has a crucial role in hydrodynamic dispersion. The movement of molecules or ions governs it and explains the process of solute diffusion from areas of high concentration to lower concentration. The MODFLOW model was used to simulate the steady-state flow of groundwater by entering model parameters.

Results and discussion

Flood risk analysis

Hydrologic analysis

The hydrology toolset extension in ArcGIS was employed to analyze and delineate flood-prone areas. Surface water movement was simulated to identify potential water sources and areas susceptible to accumulation. A flow accumulation map was generated through several steps, which included filling the Digital Elevation Model (DEM) to remove depressions and producing a flow direction map utilizing the filled DEM as input raster data (refer to Fig. 6). A coding direction was established by utilizing both the surface input raster and the raster displaying flow direction. Following the acquisition of flow accumulation results, an input stream raster was generated by applying a threshold to the outcomes. This step aids in delineating stream networks within the study area, facilitating further analysis and mapping of flood-prone regions.

For instance, a threshold value of 50 indicates that each drainage network cell has at least 50 contributing cells. As a

Table 5 Assessment parameters used in MODFLOW

Parameter	Description
Grid division	25 cells (vertical) × 20 cells (horizontal)
Region with constant head boundary	Coal mining region in the eastern section
River conductance	0.00811 m/s
Hydraulic heads	Range, 5.57 to 9.67 m
Starting head	5.57 m
Starting nitrate concentration	3.14 mg/L
Transverse dispersivity	0.85 m
Vertical dispersivity	0.085 m
Molecular diffusion coefficient	1.48608×10^{-4} m^2/day
Model used	MODFLOW
Simulation type	Steady-state flow

Fig. 5 Framework of the model
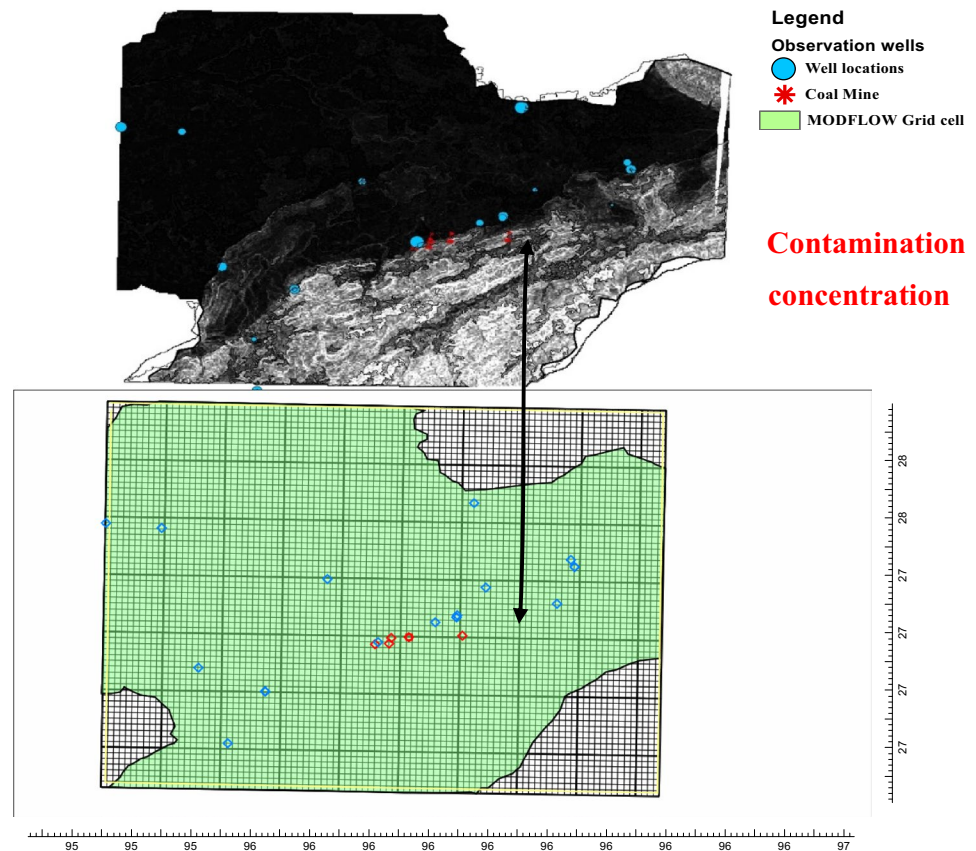
result, multiple accumulation thresholds were used to extricate the stream until a stream was attained, and the resulting stream map was utilized (Fig. 6). The buffer (coverage) surrounded input coverage features with polygons. The typical breadth of stream networks in the study location was determined to be less than 500 m. Consequently, using the stream network, a 1 km-long buffer was established. Therefore, areas within the buffer zone were deemed susceptible to flooding, and vice versa. The buffer (coverage) surrounded input coverage features with polygons. The typical breadth of stream networks in the study location was determined to be less than 500 m. Consequently, using the stream network, a 1 km-long buffer was established. Therefore, areas within the buffer zone were deemed susceptible to flooding, and vice versa.

Surface analysis

Utilizing the spatial analyst tool within ArcGIS, the Digital Elevation Model (DEM) served as the input raster data to generate a slope map. The slope tool facilitated the computation of the maximum change in elevation between each cell and its neighboring cells. Steepest descent was identified based on the most significant change in elevation between the cell and its nearest neighbors. It is pertinent to acknowledge that regions characterized by rugged terrain

and pronounced gradients typically exhibit lower susceptibility to inundation. Due to the study area's undulating nature, the resulting slope map was categorized into high, medium, and low slope areas. Areas with steep gradients are less prone to flooding, whereas those with gentler slopes are more susceptible. Subsequently, a flood-prone map was derived by integrating the slope map with the map depicting stream networks. Regions falling within a 1 km buffer zone from the stream networks and exhibiting slope values ranging from 0 to 10 were reclassified as areas bearing a very high risk of inundation (refer to Fig. 7). Additionally, certain areas beyond the 1 km buffer zone were identified as moderately susceptible to inundation.

Flood risk analysis

In summary, combining the buffered stream connection map and the slope map of the research area resulted in creating a flood danger map focused on the Margherita mining zone. The flood hazard map for the Margherita mining zone was generated using the analytical hierarchy process (AHP). The allocation of weight to various parameters was as follows: proximity to streams (25%), slope (20%), land use (15%), soil type (10%), buffered stream connection (15%), and flow direction (15%). The weights were derived based on the relative significance of each factor in affecting flood
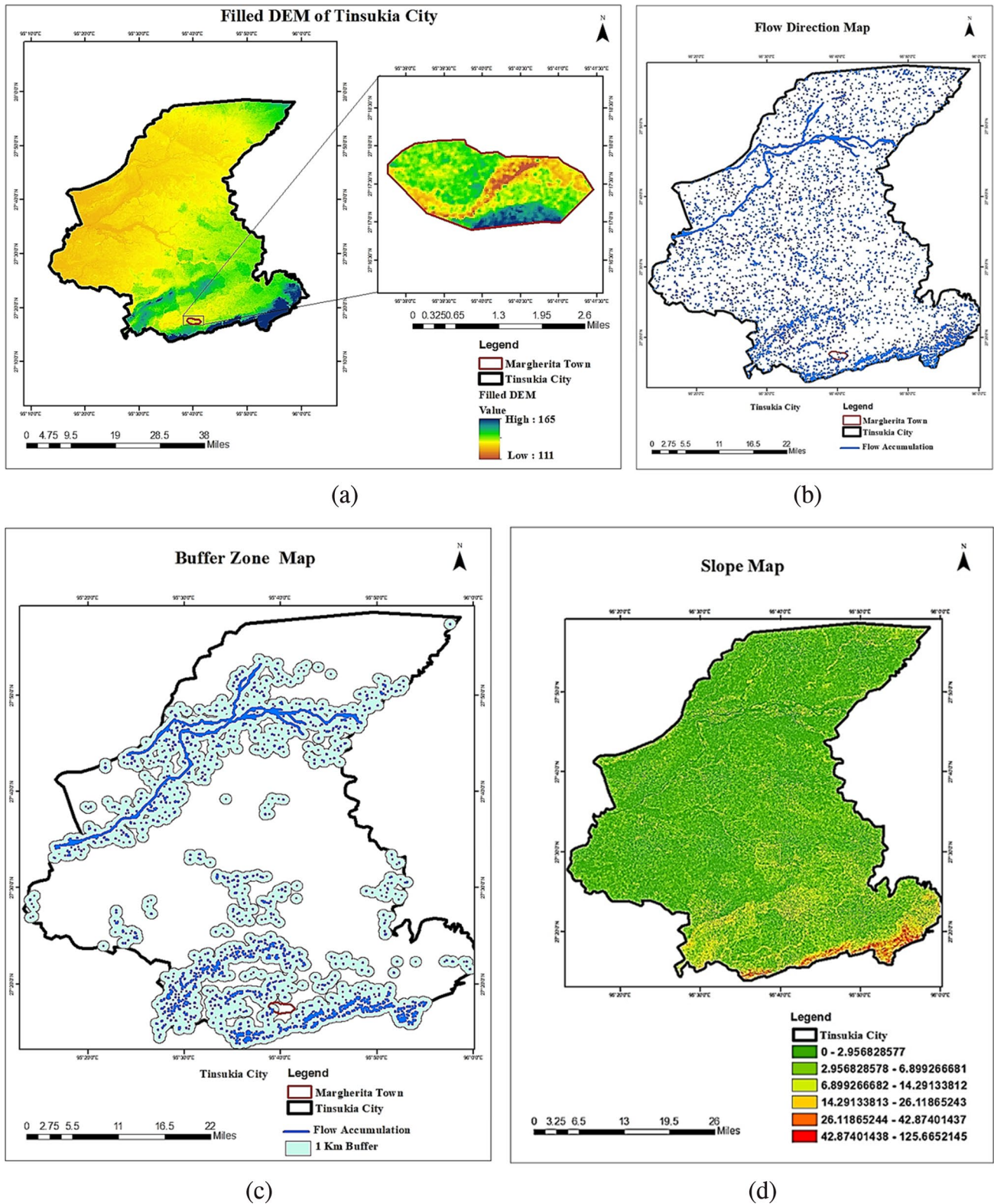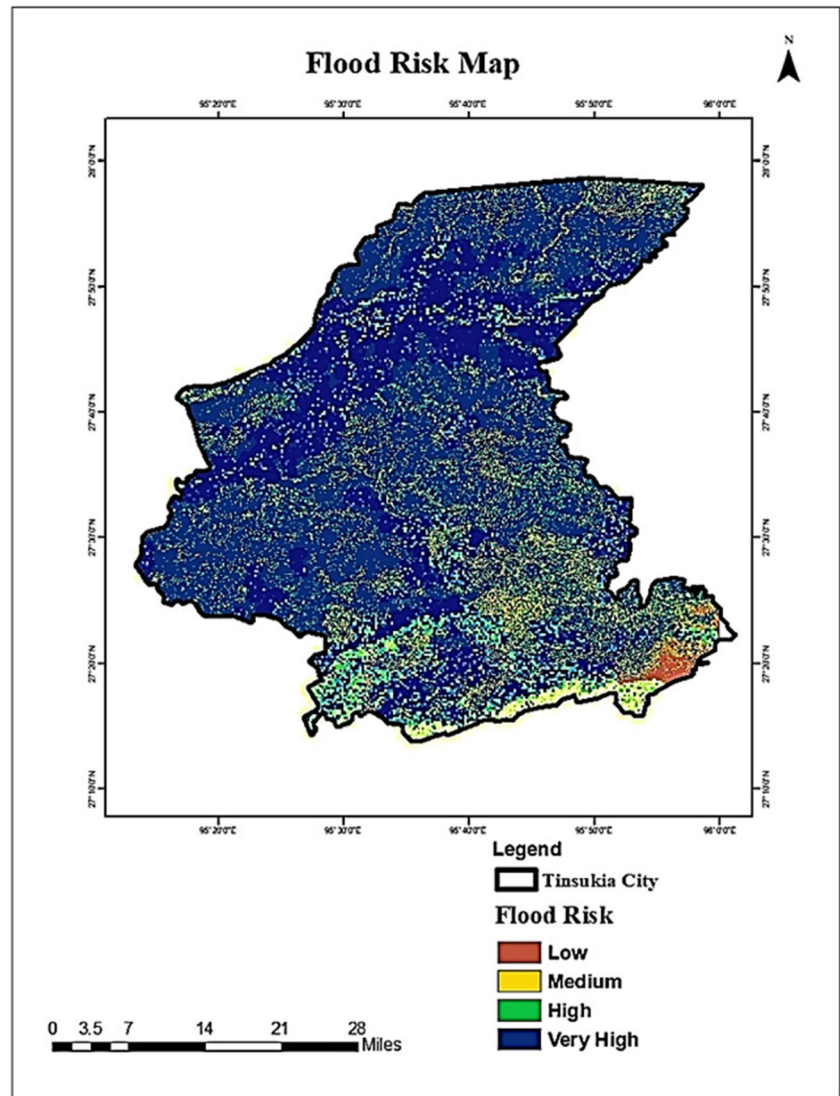
(a)

(b)

(c)

(d)

Fig. 6 **a** Hydrologic analysis (filled DEM). **b** Flow direction map. **c** Buffer zone map. **d** Slope map

Fig. 7 Flood risk map

susceptibility. The combination of these elements led to the creation of a flood hazard map that classifies places of very high, high, medium, and low sensitivity to flooding. The map indicated that about 38.08% of the research region is susceptible to floods. The map categorizes places vulnerable to flooding into four basic categories: very high, high, medium, and low flood susceptibility. The total area

occupied by the different categories was computed based on the flood-prone map (Table 6), as shown in Fig. 8. In order to produce a flood hazard map focused on the Margherita mining zone, it was necessary to integrate the buffered stream connection map and the slope map inside the study area. This was done to facilitate the process of map production. Figure 7 demonstrates the flood-prone map, which is included in Table 6, to calculate the exact area inhabited by each susceptibility group. Based on the inquiry's findings, it was discovered that about 38.08% of the land under consideration is susceptible to floods. This thorough research aims to provide significant insights into the spatial distribution of flood risk within the Margherita mining zone by presenting relevant findings. Such insights may aid in decision-making by using reliable information and applying effective management measures to minimize the risk of floods.
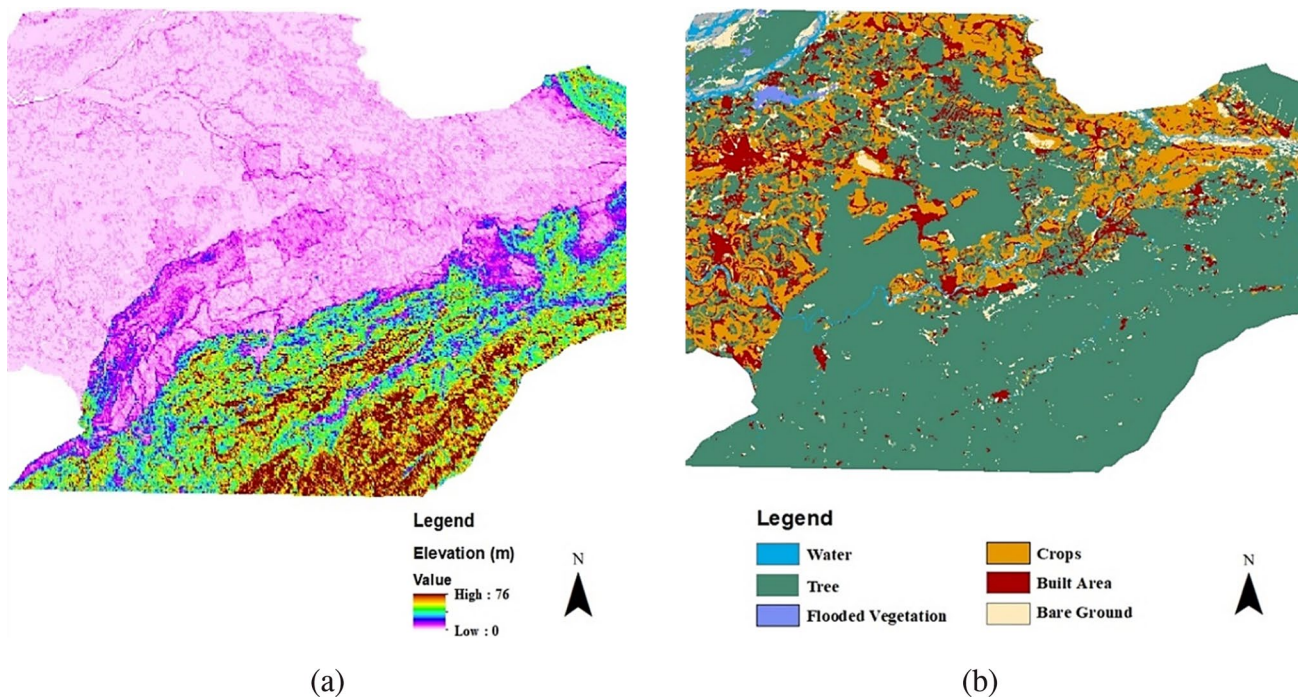
Table 6 Area distribution of flood-prone zones within the study area

Degree of flood vulnerability	Area (km^2)	Percentage (%)
Very high	521.13	13.75
High	922.11	24.33
Medium	1496.67	39.49
Low	850.09	22.43
Total	3790	100

(a)   (b)

Fig. 8 **a** Elevation map. **b** Land cover map

Assessment in MODFLOW

Effects of surface runoff and elevation

When the soil gets saturated or impermeable barriers hinder water penetration, surface runoff refers to the water flow on Earth's surface, generally after precipitation or snowmelt.

The region's topography, slope, and land cover features may all impact how surface runoff and elevation relate (Fig. 8). In most cases, elevation significantly influences surface runoff's likelihood. Elevation changes are directly correlated with changes in the topography and slope of the ground. The velocity of surface runoff may be accelerated by steeper slopes, often seen at higher altitudes. Water moves more

Fig. 9 Contamination spread according to land cover
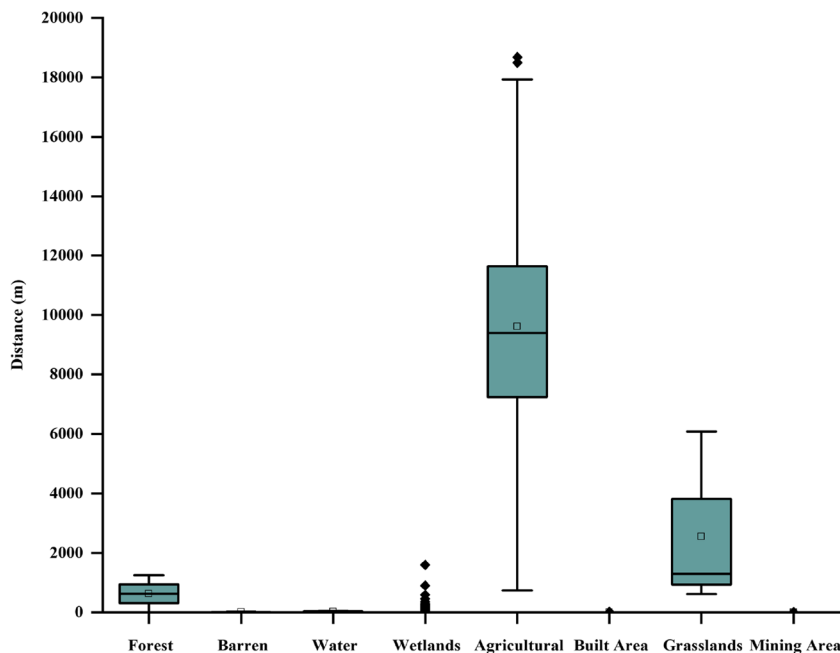
quickly and downslopes in certain regions, increasing the possibility of surface runoff formation. Elevation changes have an impact on the development of drainage patterns. Surface runoff gathers and starts downstream at higher elevations, often serving as the source regions for streams and rivers. Runoff from higher altitudes may enter lower elevations, increasing surface runoff in those places. Elevation may also have an impact on the kinds and distribution of plant and land cover, which in turn has an impact on surface runoff. Regarding the quantity of water intercepted by vegetation or absorbed by the soil, it is vital to remember that local characteristics and regional climatic trends may affect surface runoff and elevation. For a given research region, in-depth analysis and modeling employing hydrological and topographical data may provide more precise insights into the link between surface runoff and elevation.

Land use and land cover patterns are directly connected to surface water and runoff. The type, area, and land cover may greatly influence surface water runoff quantity and quality. The link between surface water runoff and land use/land cover has the following major components: Impervious Surfaces: Land uses like urban or built-up regions with a high proportion of impervious surfaces (concrete, asphalt) restrict the amount of rainwater that seeps into the ground. The amount and speed of surface runoff increase as water swiftly drains off these surfaces. Forested regions and vegetated land coverings, including grasslands or agricultural fields, may assist in catching rainwater, fostering infiltration, and minimizing surface runoff. A variety of agricultural practices, including crop rotation, tillage techniques, and irrigation, may have an impact on surface runoff.

Changes in land use, including urbanization and deforestation, can potentially change the hydrological cycle and increase surface runoff drastically. These maps classify and quantify several forms of land cover within a study region, offering insights into the geographic distribution and land use features. It is important to remember that the specific link between surface water runoff and land use/cover might change based on the regional climate, soil characteristics, and terrain.

Contamination over the land

Distance traveled through percolation refers to the vertical distance water travels through the soil profile, typically by percolation or infiltration. It measures the depth water penetrates the soil at a product's life cycle stage (Fig. 9). When evaluating the environmental effects of water usage, such as water consumption, groundwater depletion, or pollution, it is crucial to consider percolation distance. It aids in assessing the likelihood of water-related effects beyond the local region of water extraction or consumption. The impact categories represent different environmental, social, and economic elements that a product or process might impact throughout its life cycle. The quantity of water drained from the source is influenced by percolation distance, which may result in water shortage or depletion in the area. The probable repercussions of the depletion of water resources are assessed in this effect category. Contaminants carried by percolation may affect aquatic life, plants, or animals if they enter surface water bodies or other ecological systems. The impact category for ecotoxicity assesses possible toxicity on

Fig. 10 Duration of contamination spread
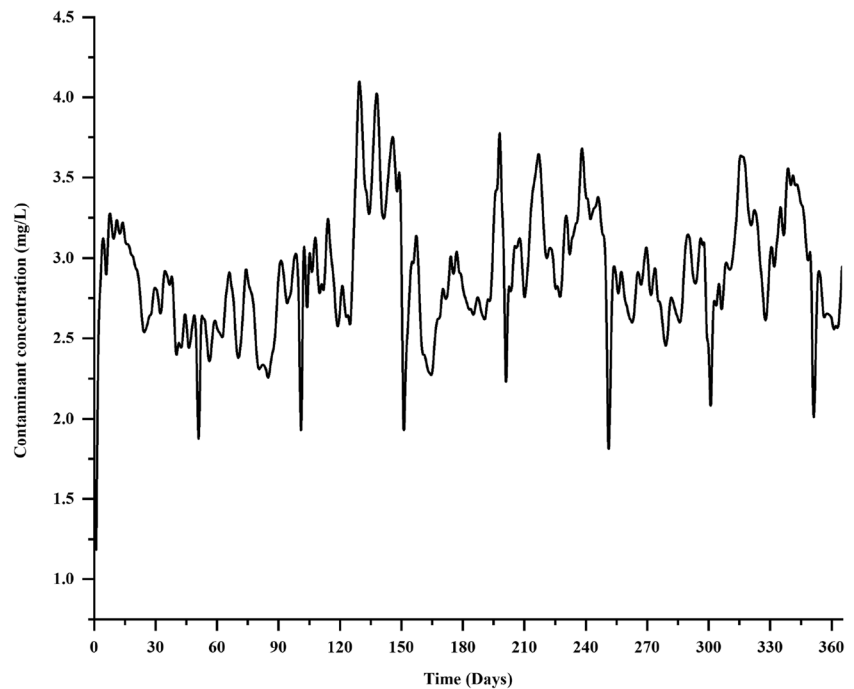
Fig. 11 Percentage % of percolation
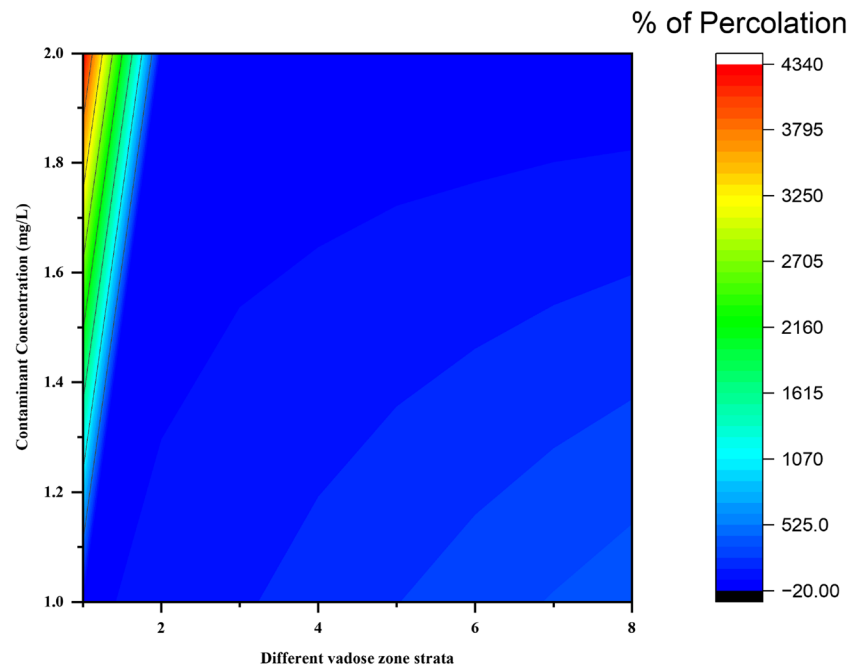
ecosystems. It is crucial to remember that the importance and severity of these impact categories might change based on regional circumstances, site-specific variables, and the particulars of the process or product being evaluated must identify and evaluate the critical impact categories linked to percolation and water-related consequences.

An illustration of how the concentration of a particular pollutant varies throughout a product's life cycle is called a contaminant concentration vs. time graph. This graph is often used to examine the environmental effects of pollutant release and dispersion at various life cycle phases (Fig. 10). This graph shows how the concentration of the contaminant varies over time as it is moved through and distributed in the environment. This knowledge may be used to evaluate the contaminant's potential for environmental exposure and its effects. By examining the pollutant concentration vs. time graph, hotspots or critical moments when the contaminant concentration reaches a peak or surpasses specific criteria may be found in the life cycle. These hotspots may guide the decision-making process for pollution prevention and control actions. It is crucial to remember that depending on the exact contamination, the kind of product or process being examined, and the environmental circumstances, the form and properties of the contaminant concentration vs. time graph might change dramatically. Therefore, undertaking a thorough and context-specific involving reliable data collection and suitable modeling methodologies is essential for effectively capturing and understanding changes in pollutant concentration over time.

percolation and contamination spread

As part of the testing and calibration process of the model, a simplified version was developed, concentrating solely on one geological formation. This focused approach allowed for a detailed examination of the system's behavior regarding various parameters and the influence of conduits on the aquifer, alongside other pertinent hydrological characteristics (Fig. 11). The simplified setup was explicitly tailored to analyze two distinct sets of recharge events: firstly, a 1-day recharge event with a magnitude of $R = 50$ mm, succeeded by a 10-day recession period; secondly, a 2-day recharge event with a magnitude of 40 mm, followed by a 15-day recession period. These simulated scenarios aimed to elucidate the response of the aquifer system to varying recharge patterns and durations, providing valuable insights into its dynamic behavior under different hydrological conditions. In addition, a specific event was examined, which had the highest recorded recharge between 2014 and 2019, measuring 60 mm. This was followed by 30 days of declining recharge.

Subsequently, detailed modeling incorporating the area's geography and geology, including the primary aquifer, was undertaken. The hydrogeological model was expanded to include a more extensive region to assess variations in the potentiometric surface related to geological characteristics and provide a more comprehensive understanding of the southern catchment border (Fig. 12). Using these models was crucial in determining the most likely karst network and precisely defining catchment borders. To improve computational efficiency and prioritize the karst aquifer, the model deliberately removed nearby geological formations, such as

the Glencar limestones and Slishwood paragneiss, that are not karstified. These deposits have hydraulic conductivities of $K = 1e^8$ and $K = 11$ m/s, respectively. The choice to exclude these formations was influenced by many variables, such as the notable differences in hydrogeological characteristics, surface watershed/topography, and high hydraulic gradients seen inside the karst aquifer.

By excluding non-karstified formations from the model, computational speed and accuracy were notably enhanced, allowing for a more focused and precise analysis of the karst network's behavior and hydrological dynamics. Figure 12 depicts various experiments to assess conduit network topologies, ranging from basic to intricate designs and shallow to deep configurations. Both steady-state (assessed through the analysis of resulting potentiometric surfaces) and transient (validated against several spring discharge events) outcomes of these experiments were meticulously examined and calibrated. The steady-state condition was initiated with a recharge rate of 0.0082 m over 365 days. The recharge rate used in the research was around three times higher than the average yearly recharge of the watershed. The computational grid included 65 rows and columns, including ten vertical levels spanned various altitudes.

Ranging from 63 to 348 m, the thickness of each layer was adjusted to accommodate geological variations. Cell dimensions were standardized at 40×40 m for the general aquifer, with smaller dimensions applied as necessary of 20×20 m around the conduits and 10×10 m utilizing quadtree grid refinement. Turbulence within the pipes was determined using the Manning equation. Conduit network configurations included round, vertical, horizontal, or angled conduits. A fixed head of 120 m was established and designated along the eastern border of the Dartry limestone formation within the catchment.

The efficiency of the conduit network was significantly improved after analyzing the geological transition from the Dartry limestones to the Glencar limestones. This change was marked by a noticeable increase in clay, as shown in Fig. 5c. Following that, it was determined that a reevaluation of the borders of the area where water is collected and
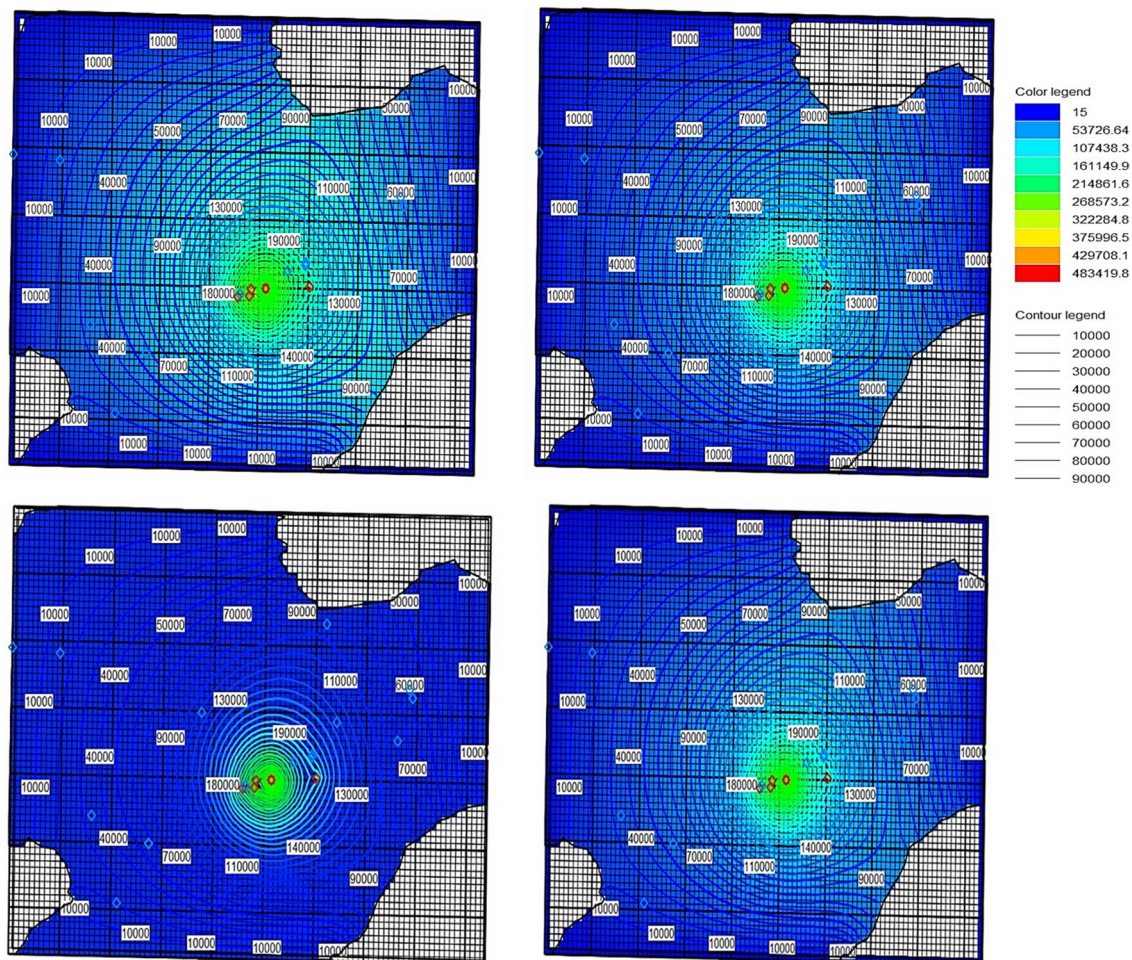

Fig. 12 Percolation and spread of contamination

the anticipated physical characteristics of the underground limestone network was required. This is shown in Fig. 6. Tracer tests, topographical data, 3D geological modeling, and groundwater flow simulations informed the determination of catchment limits. The delineation of the northern boundary was accurately guided by the geological features of the Glencar Shaley limestone formations, while a presumed plugged fissure demarcated the southeastern boundary. The likely position of the groundwater divide is identified along the southern boundary. This determination is made through a comparative analysis between the 3D geological model; the area displays a concave bending shape of the Dartry limestones and Glencar formation, together with the potentiometric surface resulting from an exceptional occurrence, which corresponds to double the highest recorded daily rainfall during periods of solid flow. The geological demarcation of the division becomes less clear near the southwest and western limits. Subsequent examination of documented karst characteristics in the surrounding region uncovered the existence of a smaller karst spring, which is linked to the Manorhamilton watershed via its drainage area. This observation suggests that the probable location of the groundwater divide aligns with the termination of this geological folding, approximately halfway between identified conduits and this neighboring catchment. Figure 7 illustrates the steady-state potentiometric surface for the optimal configuration. Before the commencement of the temporary time increments, the steady state was formed at day 365.

Conclusion

Using Digital Elevation Models (DEMs), a geographical information system (GIS) technique was employed to identify areas susceptible to flooding within the Margherita mining region. Locations near coal mining zones were carefully selected to reflect the groundwater system suitably. The MODFLOW modeling framework was employed to simulate various scenarios and assess the effects of groundwater contamination on water quality. In addition to groundwater quality concerns, the Margherita region is especially susceptible to flooding due to its high mining activities and bad land-use changes. The utilization of ArcGIS facilitated the generation of several morphological attributes derived from digital elevation models (DEMs), notably local slope and flow network analyses. Findings indicate that approximately 38.08% of the surveyed area exhibited high susceptibility to inundation. Twenty-five scenarios were simulated using MODFLOW; according to the percolation percentage and contamination, 35% of the study area, i.e., the middle of the research area, was the most affected. About 38.08% of the area around the mining

zones surrounding Margherita is prone to floods. Consequently, it is inferred that the mining environs encompassing the Margherita municipality were comparatively less prone to flooding. This study introduces a simplified methodology for delineating and assessing flood-prone regions, offering a valuable resource for flood risk mitigation, disaster preparedness, and mitigation efforts within the study area. Furthermore, an analysis of electrical conductivity (EC) and total dissolved solids (TDS) values indicates that the research area should be classified into a moderate to high salinity zone suitable for irrigation purposes. Groundwater flows towards and along the course of river movement. Therefore, pollutants are readily transported from upstream to downstream.

Declarations

Ethics approval Not applicable.

Consent to participate All authors have consented to participate in this paper.

Consent for publication All authors have consented to publish this paper.

Competing interests The authors declare no competing interests.

References

Duran L, Gill L (2021) Modeling spring flow of an Irish karst catchment using Modflow-USG with CLN. J Hydrol 597:125971. https://doi.org/10.1016/j.jhydrol.2021.125971

Esfahani SG, Valocchi AJ, Werth CJ (2021) Using MODFLOW and RT3D to simulate diffusion and reaction without discretizing low permeability zones. J Contam Hydrol 239:103777. https://doi.org/10.1016/j.jconhyd.2021.103777

Ganji K, Gharechelou S, Ahmadi A, Johnson BA (2022) Riverine flood vulnerability assessment and zoning using geospatial data and MCDA method in Aq'Qala. Int J Disaster Risk Reduct 82:103345. https://doi.org/10.1016/j.ijdrr.2022.103345

Jaxa-Rozen M, Kwakkel JH, Bloemendal M (2019) A coupled simulation architecture for agent-based/geohydrological modelling with NetLogo and MODFLOW. Environ Model Softw 115:19–37. https://doi.org/10.1016/j.envsoft.2019.01.020

Jerin T, Azad MAK, Khan MN (2023) Climate change-triggered vulnerability assessment of the flood-prone communities in Bangladesh: a gender perspective. Int J Disaster Risk Reduct 95:103851. https://doi.org/10.1016/j.ijdrr.2023.103851

Kareemuddin M, Rusthum DS (2015) Developing custom ArcGIS tools to prepare data for solar potential analysis using remote sensing data and image processing techniques. Int J Innov Technol Res 3:2519–2528

Kim B-J, Ko M-S (2023) Two-dimensional reactive transport model as a new approach for identifying the origins and contribution of arsenic in a soil and water system. Sci Total Environ 898:165468. https://doi.org/10.1016/j.scitotenv.2023.165468

Kimanzi JK, Wishitemi BEL (2001) Effects of land use changes on herbivores of Masai mara ecosystem. Int J Environ Stud 58:727–740. https://doi.org/10.1080/00207230108711364

Langlois BK, Marsh E, Stotland T, Simpson RB, Berry K, Carroll DA, Ismanto A, Koch M, Naumova EN (2023) Usability of existing global and national data for flood related vulnerability assessment in Indonesia. Sci Total Environ 873:162315. https://doi.org/10.1016/j.scitotenv.2023.162315

Lazzarin T, Viero DP, Molinari D, Ballio F, Defina A (2022) A new framework for flood damage assessment considering the within-event time evolution of hazard, exposure, and vulnerability. J Hydrol 615:128687. https://doi.org/10.1016/j.jhydrol.2022.128687

Sundar ML, Ragunath S, Hemalatha J, Vivek S, Mohanraj M, Sampathkumar V, Ansari AM, Parthiban V, Manoj S (2022) Simulation of ground water quality for Noyyal river basin of Coimbatore city, Tamilnadu using MODFLOW. Chemosphere. 306:135649. https://doi.org/10.1016/j.chemosphere.2022.135649

Jibhakate SM, Timbadiya PV, Patel PL (2023) Multiparameter flood hazard, socioeconomic vulnerability and flood risk assessment for densely populated coastal city. J Environ Manage 344:118405. https://doi.org/10.1016/j.jenvman.2023.118405

Mendoza ET, Salameh E, Sakho I, Turki I, Almar R, Ojeda E, Deloffre J, Frappart F, Laignel B (2023) Coastal flood vulnerability assessment, a satellite remote sensing and modeling approach. Remote Sens Appl: Soc Environ 29:100923. https://doi.org/10.1016/j.rsase.2023.100923

Osei BK, Ahenkorah I, Ewusi A, Fiadonu EB (2021) Assessment of flood prone zones in the Tarkwa mining area of Ghana using a GIS-based approach. Environ Challenges 3:100028. https://doi.org/10.1016/j.envc.2021.100028

Rafiei V, Nejadhashemi AP (2023) Watershed scale PFAS fate and transport model for source identification and management implications. Water Res 240:120073. https://doi.org/10.1016/j.watres.2023.120073

Sarker MNI, Alam GMM, Firdaus RBR, Biswas JC, Islam ARMT, Raihan ML, Hattori T, Alam K, Joshi NP, Shaw R (2022) Assessment of flood vulnerability of riverine island community using a composite flood vulnerability index. Int J Disaster Risk Reduct 82:103306. https://doi.org/10.1016/j.ijdrr.2022.103306

Sathe SS, Mahanta C (2019) Groundwater flow and arsenic contamination transport modeling for a multi aquifer terrain: assessment and mitigation strategies. J Environ Manage 231:166–181. https://doi.org/10.1016/j.jenvman.2018.08.057

Singh P, Singh RM (2019) Identification of pollution sources using artificial neural network (ANN) and multilevel breakthrough curve (BTC) characterization. Environ Forensics 20:219–227. https://doi.org/10.1080/15275922.2019.1629548

Sivakumar V, Chidambaram SM, Velusamy S, Rathinavel R, Shanmugasundaram DK, Sundararaj P, Shanmugamoorthy M, Thangavel R, Balu K (2022) An integrated approach for an impact assessment of the tank water and groundwater quality in Coimbatore region of South India: implication from anthropogenic activities. Environ Monit Assess 195:88. https://doi.org/10.1007/s10661-022-10598-4

Wei X, Bailey RT (2021) Evaluating nitrate and phosphorus remediation in intensively irrigated stream-aquifer systems using a coupled flow and reactive transport model. J Hydrol 598:126304. https://doi.org/10.1016/j.jhydrol.2021.126304

Wei X, Bailey RT, Records RM, Wible TC, Arabi M (2019) Comprehensive simulation of nitrate transport in coupled surface-subsurface hydrologic systems using the linked SWAT-MODFLOW-RT3D model. Environ Model Softw 122:104242. https://doi.org/10.1016/j.envsoft.2018.06.012

Xing Z, Yang S, Zan X, Dong X, Yao Y, Liu Z, Zhang X (2023) Flood vulnerability assessment of urban buildings based on integrating high-resolution remote sensing and street view images. Sustain Cities Soc 92:104467. https://doi.org/10.1016/j.scs.2023.104467

You X, Liu S, Esfahani SG, Duan Y, Li J, Dai C, Werth CJ (2023) Modeling EDTA-facilitated cadmium migration in high- and low-permeability systems using MODFLOW and RT3D. J Contam Hydrol 256:104171. https://doi.org/10.1016/j.jconhyd.2023.104171

Zhang K, Shalehy MH, Ezaz GT, Chakraborty A, Mohib KM, Liu L (2022) An integrated flood risk assessment approach based on coupled hydrological-hydraulic modeling and bottom-up hazard vulnerability analysis. Environ Model Softw 148:105279. https://doi.org/10.1016/j.envsoft.2021.105279

Zhao C, Li M, Wang X, Liu B, Pan X, Fang H (2022) Improving the accuracy of nonpoint-source pollution estimates in inland waters with coupled satellite-UAV data. Water Res 225:119208. https://doi.org/10.1016/j.watres.2022.119208